

# 微合金 EH40 型船板钢大热输入焊接 接头组织和力学性能

孙 占<sup>1</sup>, 黄继华<sup>1</sup>, 张 华<sup>1</sup>, 赵兴科<sup>1</sup>, 李曲全<sup>2</sup>

(1. 北京科技大学 材料科学与工程学院, 北京 100083;

2. 湘潭钢铁集团, 湖南 湘潭 450051)

**摘 要:** 通过拉伸、冲击、硬度力学试验和接头微观组织分析, 对 EH40 船板钢大热输入埋弧焊的焊接性和接头性能进行了试验分析。结果表明, 以热输入为 40 kJ/cm 和 60 kJ/cm 焊接, 焊接热影响区粗晶区冲击吸收功值均最低, 分别为 116 J 和 80.5 J; 焊接接头的强度均高于母材, 焊接热影响区均未出现焊接软化区。当焊接热输入为 40 kJ/cm 时, 粗晶区组织主要为板条贝氏体、粒状贝氏体、少量的块状铁素体, 而焊接热输入为 60 kJ/cm 时, 板条贝氏体明显减少, 块状铁素体增多, 并出现少量针状铁素体。Ti、Nb 合金元素的碳氮化合物第二相粒子, 在大焊接热输入时, 很大程度上阻止粗晶区奥氏体晶粒的长大, 改善了该区域的冲击性能。

**关键词:** 船板钢; 组织; 第二相粒子; 大热输入

**中图分类号:** TG457 **文献标识码:** A **文章编号:** 0253-360X(2008)03-0041-04



孙 占

## 0 序 言

随着国内造船业的迅速发展, 造船的技术水平也取得了长足的进步, 造船工业向大型化、轻型化方向发展, 高强度、高质量 E、F 级船板钢的应用比例正在不断提高。新一代 EH40 船板钢是在低碳及低硫的基础上, 添加 Nb、Ti、Ni、Mo、V 等合金元素, 并结合控轧控冷(TMCP)等形变热处理技术, 从而获得的一种细晶粒高强度微合金钢。

焊接是造船的关键技术, 焊接接头性能的好坏直接影响整个船体的质量。以往通常采用小热输入的多层多道焊来改善该区域的组织及韧性。随着对焊接生产效率要求的不断提高, 往往采用大热输入焊接, 如单面埋弧焊(SAW)、气电焊(EGW)及电渣焊(ESW)等焊接技术。大热输入焊接时, 峰值温度升高, 高温停留时间延长, 出现严重的晶粒长大, 使焊接热影响区(HAZ)相对原始母材发生很大变化, 造成 HAZ 的脆化和软化<sup>[1]</sup>。这无疑对船体结构用钢的可焊性和制定合理的焊接工艺提出了更高的要求。因此, 研究其裂纹敏感性和焊接 HAZ 的力学性能, 分析 EH40 船板钢焊后组织和焊接性能特点, 对 EH40 船板钢得到广泛的应用无疑具有重要的工程

实际意义。

## 1 试验方法

试验用钢为新型 EH40 船板钢, 由于采用 TMCP 技术和低碳微合金强化处理, 钢板组织主要为铁素体和部分珠光体, 其化学成分如表 1 所示。焊接试验采用多层多道埋弧焊对接, 钢板尺寸为 500 mm×200 mm×40 mm, 开双 Y 形坡口, 如图 1 所示。焊接材料为 H10Mn2+SJ101, 焊丝规格为  $\phi 5.0$  mm, 焊前预热 50 °C, 道间温度控制在 150 °C, 两次对接试验的焊接热输入分别为 40 kJ/cm 和 60 kJ/cm。

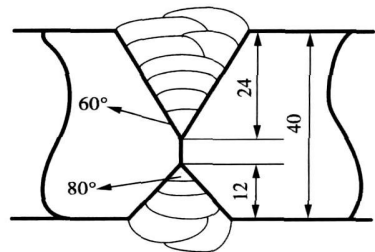


图 1 埋弧焊焊接工艺示意图 (mm)

Fig. 1 Diagrammatic sketch of welded joint in submerged arc welding procedure

表 1 EH40 船板钢的化学成分(质量分数, %)  
Table 1 Chemical composition of EH40 ship steel plate

C	Si	Mn	Al	P	S	Nb	Ti	Ni	C <sub>eq</sub> *	P <sub>cm</sub> *
0.100	0.370	1.470	0.023	0.020	0.001	0.025~0.032	0.010~0.015	0.120~0.145	0.354	0.182

注: C<sub>eq</sub> = C + Mn/6 + (Cr + Mo + V)/5 + (Ni + Cu)/15; P<sub>cm</sub> = C + Si/30 + Mn/20 + Cu/20 + Ni/60 + Cr/20 + Mo/15 + V/10 + 5B

焊后对焊接接头进行拉伸、冲击和硬度力学试验,用扫描电镜分析冲击断口形貌,利用光学显微镜和透射电镜对焊接接头不同区域进行微观组织和第二相粒子分析,腐蚀溶液采用 3%硝酸酒精。焊接接头冲击试验采用 V 形缺口,取样部位如图 2 所示。冲击试验位置分别为焊缝、熔合线和距离熔合线 2 mm 和 4 mm 处(图 2 中 A, B, C, D 位置),每个位置取 3 个试样的试验结果求平均值,冲击试验温度为 -20 °C。

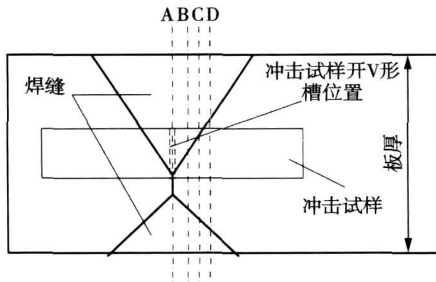


图 2 焊接接头冲击试样取样示意图

Fig. 2 Position of impact test samples from welded joint

## 2 焊接接头力学性能

### 2.1 冲击性能

从表 2 冲击试验结果来看,两种热输入焊接后,焊接热影响区中熔合线附近的粗晶区冲击吸收功值均最低(116, 80.5 J),但均为韧性和准解理混合断裂,随着远离熔合线距离的增加,冲击吸收功值都有增加的趋势,距离熔合线 4 mm 处的冲击吸收功值跟母材接近。

表 2 EH40 船板钢焊接接头冲击试验结果(冲击吸收功 A<sub>KV</sub>/J)

Table 2 Results of impact test for EH40 ship steel plate						
焊接热输入 E/(kJ·cm <sup>-1</sup> )	冲击温度 T/°C	距熔		距熔		母材
		焊缝	熔合线	合线 2 mm	合线 4 mm	
40	-20	97	116	186	218	217~259
60		70	85	185	246	

### 2.2 拉伸性能

由于试验钢板强度高,也比较厚,根据船级社拉伸试验规定,分别沿焊缝的上下表面取样,试样厚度 25 mm,以 2 个试样试验结果的算术平均值作为整个接头的试验结果。拉伸试验力学性能结果如表 3 所示。

表 3 EH40 船板钢的拉伸性能

Table 3 Tensile test results of for EH40 ship steel plate

焊接热输入 E/(kJ·cm <sup>-1</sup> )	屈服强度 R <sub>eL</sub> /MPa			抗拉强度 R <sub>m</sub> /MPa			断后伸长率 A(%)	断裂 位置
40(试板 1)	475	480	495	572	576	580	22~24	母材
	483			576				
60(试板 2)	591	470	585	582	573	579	23~25	母材
	482			578				
母材	455~520			545~600			22~25	—

拉伸试验中焊接接头的断口均位于母材区,表明整个焊接接头强度高于母材,没有出现软化现象。拉伸过程中无明显的屈服平台,呈现为连续屈服现象,这与 EH40 船板钢的母材组织有很大关系,其基体由多边形铁素体、针状铁素体和部分珠光体组成,具有高密度的可移动位错,易于实现多滑移。这与拉伸试验时,断口位置远离接头现象相符。

## 3 焊接热影响区组织分析

焊接时,距焊缝不同距离的点受到不同峰值温度焊接热循环的影响,组织发生不同的转变,依次可以将热影响区分为粗晶区、细晶区和不完全相变区。结合冲击试验结果发现,焊接接头熔合线附近的粗晶热影响区是焊接接头中韧性最差的一个区域。

焊接大热输入作用下,靠近熔合线的母材重新奥氏体化,发生新的二次组织转变,母材(图 3a)原有的轧制组织及分布完全消失,粗大的奥氏体晶界清晰可见。图 3b, c 为 EH40 船板焊接粗晶区的光学显微组织,以 40 kJ/cm 的热输入焊接时,冷却时间 t<sub>8/5</sub> = 25 s,奥氏体晶粒约为 25 μm(普通低碳钢焊接后奥氏体晶粒在 100 μm 以上),粗晶区组织主要为板条贝氏体和部分粒状贝氏体,另外还有少量的块状

铁素体及黑色第二相 M - A 组元,如图 3b 所示。以 60 kJ/cm 的热输入焊接时,  $t_{8/5} = 40$  s, 奥氏体晶粒约为

40  $\mu\text{m}$ , 板条贝氏体明显减少, 粗大块状铁素体增多, 并出现少量针状铁素体, 如图 3c 所示。

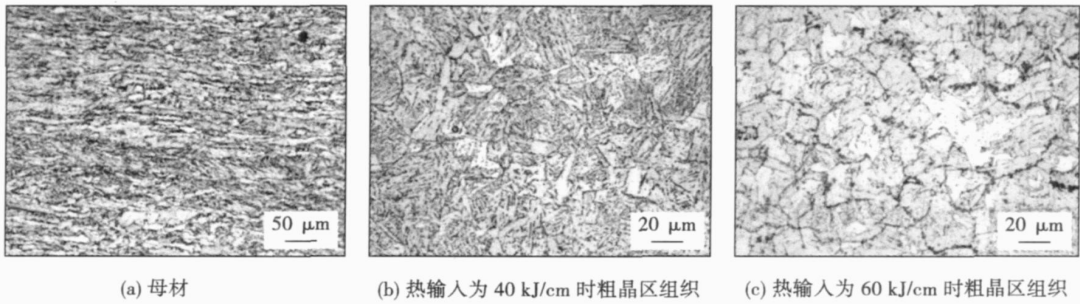


图3 母材和粗晶热影响区微观组织

Fig. 3 Microstructures of base metal and coarse grain heat affected zone

利用透射电镜对制取的碳膜复型试样进行分析, 可见 EH40 船板钢中含有大量的第二相粒子, 大多数接近球形和正方形, 粒子尺寸在 30 ~ 50 nm, 如图 4a 所示。图 4b 为焊接 ( $E = 60$  kJ/cm) 粗晶热影响区粒子分布及形貌, 可见经历焊接热循环后, 粒子数量减少且尺寸增大, 粒子形状也大部分变为方形。图中大粒子 C 元素能谱分析和衍射光斑表明, 粒子中含有 Ti 及 Nb (图中的 Cu 元素谱线来自于支持碳

膜的铜网) 两种微合金元素, 粒子为面心立方结构。因此, 可断定这些粒子为 Ti 及 Nb 合金元素的碳氮化合物。由此可见, 经焊接热循环后, 焊接粗晶区热影响区中仍能保留较多的第二相粒子, 它们在整个焊接热循环过程中能够有效钉扎奥氏体晶界, 阻止奥氏体晶粒长大<sup>[2-4]</sup>, 使得奥氏体晶粒尺寸随冷却时间增加而长大的幅值减小。

焊接接头的力学性能与其组织状态是密切相关

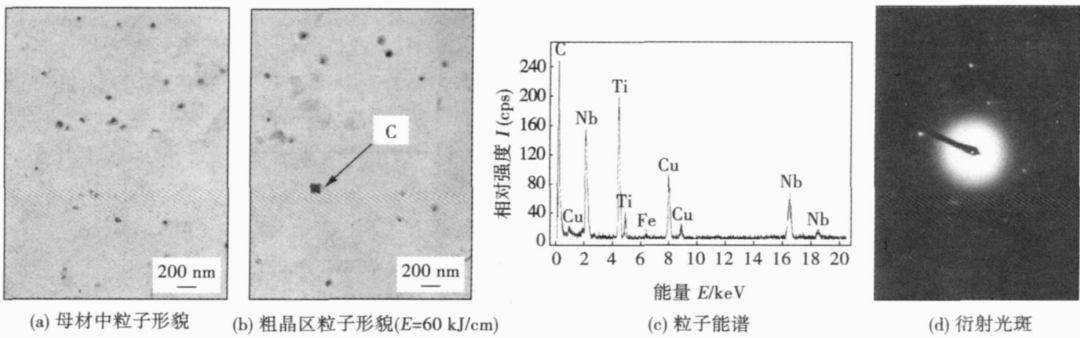


图4 母材和粗晶区中的第二相粒子

Fig. 4 TEM morphology, EDS and EDP of particles in base metal and coarse grain heat affected zone

的, 粗晶区的韧性好坏很大程度上取决于原始奥氏体晶粒尺寸和二次显微组织。板条贝氏体中的铁素体分布具有明显的方向性, 其间定向分布的 M - A 组元易诱发裂纹并为裂纹提供扩展通道, 因此其韧性较低。针状铁素体是中温转变产物, 相变温度处于晶界铁素体与贝氏体之间, 板条内的位错密度是各类铁素体中最高的, 而且它的高能量大角度晶界能够较好地阻止裂纹扩展, 一些研究表明,  $Ti_xNb_{1-x}(C_yN_{1-y})$  可以促进针状铁素体析出和 M - A 组元的分解<sup>[5]</sup>。

### 4 焊接接头的硬度

垂直切断焊缝取样, 进行抛光, 在维氏硬度试验机上对焊接接头进行硬度测试, 考虑压痕直径大小、邻近测点之间的距离和各个区域组织晶粒大小, 选择了 29.4 N 载荷。图 5 中的硬度测试结果表明, 焊接热输入为 40 kJ/cm 和 60 kJ/cm 时, HAZ 的最高硬度出现在粗晶区靠近熔合线处, 其值分别为 235 HV 和 238 HV, 从试验结果来看没有出现明显的焊接软

化区。在显微镜下测定其组织分布状态,焊接热输入为  $40 \text{ kJ/cm}$  和  $60 \text{ kJ/cm}$  时,热影响区各区宽度分别为粗晶区约  $1.3, 2 \text{ mm}$ ,细晶区约  $1.5, 2.5 \text{ mm}$ ,不完全相变区约  $1.4, 2 \text{ mm}$ ,热影响区的总长度分别为  $4.2, 6.5 \text{ mm}$  左右。

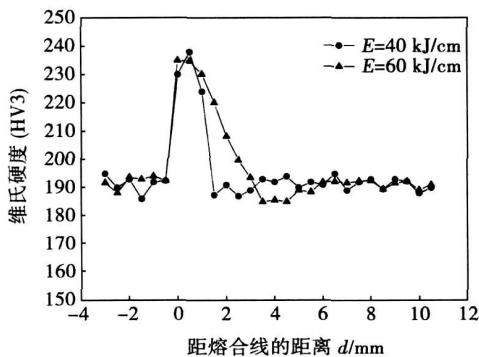


图 5 焊接接头硬度分布

Fig. 5 Distribution of hardness in welded joint

为了进一步分析粗晶区的显微组织,在该区域做显微维氏硬度  $\text{HV}0.1$  试验,测量的最高硬度值为  $265 \text{ HV}$ ,推断此区域存在少量  $\text{M}-\text{A}$  组元,出现了板条贝氏体和粒状贝氏体组织,但是其远远小于  $350 \text{ HV}$ ,说明生成的马氏体很少,此结果与显微组织照片结果相符合。

## 5 结 论

(1) 焊接接头拉伸断口位置离焊接接头较远,表明 EH40 船板钢在焊接热输入为  $40 \text{ kJ/cm}$  和  $60 \text{ kJ/cm}$  的焊接条件下,没有出现焊接热影响区软化现象。

(2) 粗晶热影响区显微组织分析表明,当焊接热输入为  $40 \text{ kJ/cm}$  时,粗晶区组织主要为板条贝氏体、粒状贝氏体、少量的块状铁素体和黑色第二相  $\text{M}-\text{A}$  组元;当焊接热输入为  $60 \text{ kJ/cm}$  时,板条贝氏体明显减少,块状铁素体增多且比较粗大,并出现少量针状铁素体。

(3) 焊接热循环作用后,粗晶区仍存在大量  $\text{Ti}$ ,  $\text{Nb}$  元素的碳氮化合物第二相粒子,它们有效阻止了奥氏体晶粒的长大,一定程度上改善了该区域的低温冲击韧性。

(4) 以热输入  $40 \text{ kJ/cm}$  和  $60 \text{ kJ/cm}$  焊接后,热影响区的最高硬度均出现在靠近熔合线的粗晶区,其值分别为  $235 \text{ HV}$  和  $238 \text{ HV}$ ,热影响区的总宽度分别为  $4.2, 6.5 \text{ mm}$ 。

## 参考文献:

- [1] 李午申. 我国合金结构钢的新发展及其焊接性[J]. 焊接学报, 2001, 22(5): 82-86.
- [2] 陈茂爱, 武传松, 王建国. 含  $\text{Ti}$  微合金钢中的第二相粒子对焊接粗晶热影响区组织及韧性的影响[J]. 焊接学报, 2002, 23(3): 37-40.
- [3] 姚 舜, 楼松年, 石忠贤. X-60 微合金钢的焊接接头韧性[J]. 上海交通大学学报, 2000, 34(12): 1622-1625.
- [4] Wang G R. Microalloying addition and fracture toughness in HSLA steels[J]. Welding Journal, 1990, 69(1): 15-22.
- [5] 元效刚, 陈茂爱, 陈俊华.  $\text{Ti}-\text{Nb}$  微合金钢焊接粗晶热影响区组织及韧性[J]. 金属成形工艺, 2004, 22(1): 30-33.

作者简介: 孙 占,男,1982 年出生,硕士研究生。主要从事微合金高强钢焊接性研究工作。发表论文 2 篇。

Email: sunzhan-237@163.com

And the mathematic model and diagrams between independent variables and functions are presented. They indicate that the effects of many coating ingredients on the slag detachability are in the mutual form. The mutual effects between  $\text{CaCO}_3$  &  $\text{BaCO}_3$ , wollastonite & AFMg powder, and rutile & iron powder increase the slag detachability separately. While the mutual effects between Al-Mg powder & fluorite, and AFMg powder &  $\text{BaCO}_3$  decrease the slag detachability separately.

**Key words:** basic electrode; slag detachability; uniform design

#### Low temperature toughness of ultra low carbon 9Ni steel welded joints

WANG Guoping, CHEN Xuedong, WANG Bing (School of Materials Science and Engineering, Hefei University of Technology, Hefei 230009, China). p37–40

**Abstract:** This article investigates the low temperature toughness of welded joints and simulated HAZ of ultra low-carbon 9Ni steel which developed by quenching, intermediate quenching and tempering processes. The specimens were investigated by Charpy V-notch impact test, optical microscope, TEM and SEM. The results show that the microstructure of lath martensite is coarsened and the low-temperature toughness is decreased in coarse grained HAZ of specimens single pass welding thermal cycled. The reversal austenite on boundaries of lath martensite appears in the dispersed distribution, and the grain will be fined, and low temperature toughness will be increased in HAZ of specimens multi-pass welding thermal cycled. It is desirable that low-heat input, multi-pass welding and low inter-pass temperature should be applied, which gives high low-temperature toughness of welded joints.

**Key words:** 9% nickel steel; thermal simulation; welded joint; low temperature impact toughness

#### Microstructures and mechanical properties of joints of microalloyed EH40 ship steel plate with high heat input welding

SUN Zhan<sup>1</sup>, HUANG Jihua<sup>1</sup>, ZHANG Hua<sup>1</sup>, ZHAO Xingke<sup>1</sup>, LI Ququan<sup>2</sup> (1. School of Materials Science and Engineering, Beijing University of Science and Technology, Beijing 100083, China; 2. Xiangtan Iron and Steel Corporation, Xiangtan 450051, Hunan, China). p41–44

**Abstract:** The weldability of EH40 ship steel plate by submerged-arc welding with high heat-input was studied by the tensile test, impact test, hardness test and microstructure. Experiment results show that the impact absorbing energy value were 116 J and 80.5 J in the coarse grain zones with the high heat-input 40 kJ/cm and 60 kJ/cm. The strength of the welded joint was better than the one of the base metal and there wasn't soft zone in HAZ. The main macrostructures were lath bainite, granular bainite and a few block-like ferrite in the coarse grain heat affected zone with 40 kJ/cm, while less lath bainite and more block-like ferrite and a few acicular ferrite appear in the some zone with 60 kJ/cm. The toughness in the coarse grain heat affected zone is improved for the existing carbides and nitrides of Ti and Nb, which prohibit the original austenite grain

from coarsening in high heat-input.

**Key words:** ship steel plate; microstructure; second phase particle; high heat-input

#### Acicular ferrite microstructure of weld metal for low-alloy steel

HUANG Anguo<sup>1</sup>, YU Shengfu<sup>1</sup>, XIE Mingli<sup>1</sup>, LI Zhiyuan<sup>1</sup>, ZHANG Guodong<sup>2</sup> (1. School of Materials Science and Engineering, Huazhong University of Science and Technology, Wuhan 430074, China; 2. College of Power and Mechanical Engineering, Wuhan University, Wuhan 430072, China). p45–48

**Abstract:** For understanding the microstructure acicular ferrite (AF), the thermal simulation test of weld metal in X70 pipe-line steel was carried out with GLEEBLE 1500. SEM and TEM were used to analysis the relations between the inclusions and the AF, and the C concentration distribution along AF boundary and the characteristics of sympathetic AF suffered from secondary heat cycling. The results show that there exists a layer of thin C-riched film along the AF boundary, and both the shear mechanism and the C diffusion were occurred during AF growth. The sympathetic AF nucleated on the site of high density dislocation of the primary AF and grown into specific size rapidly. Both the AF and sympathetic AF were nucleated and grown-up in the austenite grain, and were good to fine-grained strengthening effect in the multi-pass weld metal and HAZ.

**Key words:** low-alloy steel; weld metal; acicular ferrite; microstructure

#### Review of 9% Ni steel and its weldability

YAN Chunyan<sup>1</sup>, LI Wushen<sup>1</sup>, XUE Zhenkui<sup>2</sup>, BAI Shiwu<sup>2</sup>, FENG Bin<sup>2</sup> (1. School of Materials Science and Engineering, Tianjin University, Tianjin 300072, China; 2. Petroleum-Gas Pipeline Research Institute of China, Langfang 065000, Hebei, China). p49–52

**Abstract:** Research and development status of 9% Ni steel for cryogenic liquefied natural gas storage tanks were summarized and reviewed. Microstructures, mechanical properties and field weldability were presented. Most commonly used quenched and tempered 9% Ni steel is composed of a majority of tempered martensite and a few scattered retained austenites. Base metal of 9% Ni steel shows high strength, good cryogenic toughness, excellent field weldability and low cold-cracking susceptibility. Hot-cracking can be avoided under proper welding parameters. A heat input of 7–35 kJ/cm and a interpass temperature lower than 100 °C are generally adopted for the welding of 9% Ni steel.

**Key words:** liquefied natural gas storage tanks; 9% Ni steel; microstructure; welding parameters; weldability

#### Brazing between high purity alumina ceramic and oxygen-free copper

LI Feibin, WU Aiping, ZOU Guisheng, REN Jialie (Department of Mechanical Engineering, Tsinghua University, Beijing 100084, China). p53–56

**Abstract:** The joints of high purity alumina ceramic and oxygen-free copper with high strength and low gas leakage are needed in electron tube. This work investigates the effects of brazing tempera-